Volume 1 | Number 1 | Jan 2013 | Pages 1–100

Nanoscale

www.rsc.org/nanoscale

ROYAL SOCIETY OF CHEMISTRY

ROYAL SOCIETY OF CHEMISTRY

www.rsc.org/nanoscale

Nanoscale

ARTICLE

Semimetallic Molybdenum Disulfide Ultrathin Nanosheets as an Efficient Electrocatalyst for Hydrogen Evolution

Xu Sun, [a] Jun Dai, [b] Yuqiao Guo, [a] Changzheng Wu, [a] * Fanting Hu, [a] Jiyin Zhao, [a] Xiaocheng Zeng [b] and Yi Xie [a]

Molybdenum disulfide (MoS_2) ultrathin nanosheets as a well-known inorganic two dimensional (2D) material with graphene-like structure has attracted tremendous attention due to its unique microscopic and macroscopic properties brought by the confinement of charge and heat transfer upon the basal plane. However, as the prototype Mott-insulator, its relatively low conductivity and carrier concentration still greatly hamper its wide applications. Here, we developed a novel intralayer vanadium-doping strategy to produce semimetallic vanadium-doped MoS_2 (VMS) ultrathin nanosheets with less than 5 S-(V, Mo)-S atomic layers, as a new inorganic 2D material. By intralayer vanadium atoms incorporation, fine regulation of intrinsic electrical properties within the pristine MoS_2 structure has been successfully realized, achieving semimetallic MoS_2-based 2D materials with tunable conductivity and higher carrier concentration for the first time. Benefited from the enhanced in-plane conductivity, improved carrier concentration as well as the shortened electron transfer paths, the semimetal-like VMS nanosheet brought an enhanced catalytic activity with the overpotential of 0.13 V and a smaller Tafel slope, exhibiting enhanced catalytic performance than that of pure MoS_2 system. The intralayer doping in 2D structure opens a new avenue in building high efficient catalysts through the regulation of their intrinsic electrical properties, and also gives new perspective for enlarging the design space of 2D materials.

Introduction

Hydrogen energy has attracted tremendous attention for its unique superiorities as it is clean and sustainable, benefiting its status as the substitution of fossil fuels which are expensive and environmentally hazardous.[1] Great efforts have been carried out for the implementation of quantity production of this new energy carrier, among which hydrogen evolution from the electrolysis of water is the most remarkable as the water is abundant and contains no carbon contaminant.[2] During this process, the advanced catalysts such as the noble Pt-group metals[3] are often incorporated into the electrode to promote the hydrogen evolution reaction (HER), in that the proper hydrogen binding energies enabled them to catalyze the reaction at nearly zero overpotential with a fast dynamics.

Since the active centers of nature nitrogenase enzymes whose function is to fix ammonia and co-evolve hydrogen are usually metal atoms bonded to sulfur, transition-metal dichalcogenides (TMDs) have attracted increasing attentions as substitutes for traditional Pt-group metals that are expensive and scarce.[4] Molybdenum disulfides (MoS_2), a representative TMD with marginal edges as active sites,[5] is considered as one of the most promising candidates, in that Density Functional Theory (DFT) calculations have proven that the hydrogen binding energy of MoS_2 is just close to Pt-group metals in the volcano curve[6] (Figure S1). To achieve an ideal catalytic activity of MoS_2, skeleton structure design has been widely employed to achieve more edge atoms as the active sites as well as to improve the charge transferring coefficient. For example, the mesoporous MoS_2 architecture,[7] the nanostructures of single layer MoS_2

nanosheet with noble metal metals,[8] the vertically aligned layers of MoS_2,[9] as well as the defective MoS_2 nanosheets decorated with Au nanoparticles[10] have been synthesized with enhanced electrocatalytic efficiency due to the increasing fraction of edge sites. Also, for a purpose of conquering the intrinsic low conductivity and promoting the electron transfer, various hybrid structures based on MoS_2 have been designed, such as MoS_2/rGO composite,[11] the assembled structure of MoS_2 nanoparticals on Au electrode[12] as well as the exfoliated 1T-MoS_2/graphite catalysts[13]. All these hybrid structures exhibited an enhanced catalytic activity benefited from the synergistic effects between MoS_2 and the conducting matrix materials. From this viewpoint, besides hybrid structures as described above, the realization of high electrical conductivity and carrier concentration in the MoS_2 basal plane would also bring about advanced catalytic efficiency, in that the quantum-mechanical calculations revealed that the metallic edges are of significant importance for enhancing the electrocatalytic activity.[6a,14] Hence, precise modulation of electrical properties based on stable MoS_2 system toward optimized intrinsic physical properties is of great importance for the fascinating application of MoS_2 as an electrocatalyst.

Of note, inorganic 2D materials with single or few-atomic layers,[15] provide an ideal material platform for tuning the intrinsic electrical properties due to the distinctive properties brought by the 2D confinement effect.[16] As for MoS_2 nanosheet, the external applied voltage would induce the internal electrical fields in the interface area[17], which promotes the transition from a Mott-insulator to a superconductor[18]. Meanwhile, profited by the injected electrons into S-Mo-S layers from the intercalated alkaline ions, the M_xMoS_2 nanosheet (M = Li, Na, K et al.) behaves metallic behavior,[19]

even superconducting at cryogenic conditions.[20] However, the phase transition from the stable 2H-MoS_2 to 1T-MoS_2 happened as well among with the insertion of alkaline ions;[21] and the metallic 1T-MoS_2 is a thermodynamically metastable phase that is easy to turn back to Mott-insulator 2H-MoS_2 upon heating at moderate temperatures (~200 $^{\circ}$C) or aging at air conditions.[22] As a fact, the present conducting MoS_2-based systems could not be independently employed in the solution conditions due to the request of external electrical filed or the chemical instability, and thus modulating the intrinsic physical properties of MoS_2 ultrathin nanosheets within pristine 2D stable structure for improving catalytic activity is still a great challenge.

Although the MoS_2 lattice frameworks show prospective signs in catalytic applications, in-depth investigations have been significantly neglected for precisely regulating the electronic structure of MoS_2 nanosheets and even for understanding the atomic-scale relationship between the intrinsic physical property modulation and the catalytic activity. And in effect, so far the stable metallic or semimetallic MoS_2 ultrathin nanosheet has not been realized yet during the past few years. Inspired by the innovative functionality of vanadium-based composite,[23] DFT calculations (Fig. 1a and b) have evidenced that the intralayer vanadium doping in MoS_2 system would introduce the defect states with small energy differences between the defect states and the top of valence band, making the valence electrons easy to be activated to the defect states behaving as a semimetal. Herein, we highlight the intralayer vanadium doping strategy to successfully regulate the intrinsic physical properties within pristine 2H-MoS_2 structure. The vanadium doped MoS_2 (VMS) ultrathin nanosheets with less than 5 S-(V, Mo)-S atomic layers, as a new 2D material, brought the intriguing
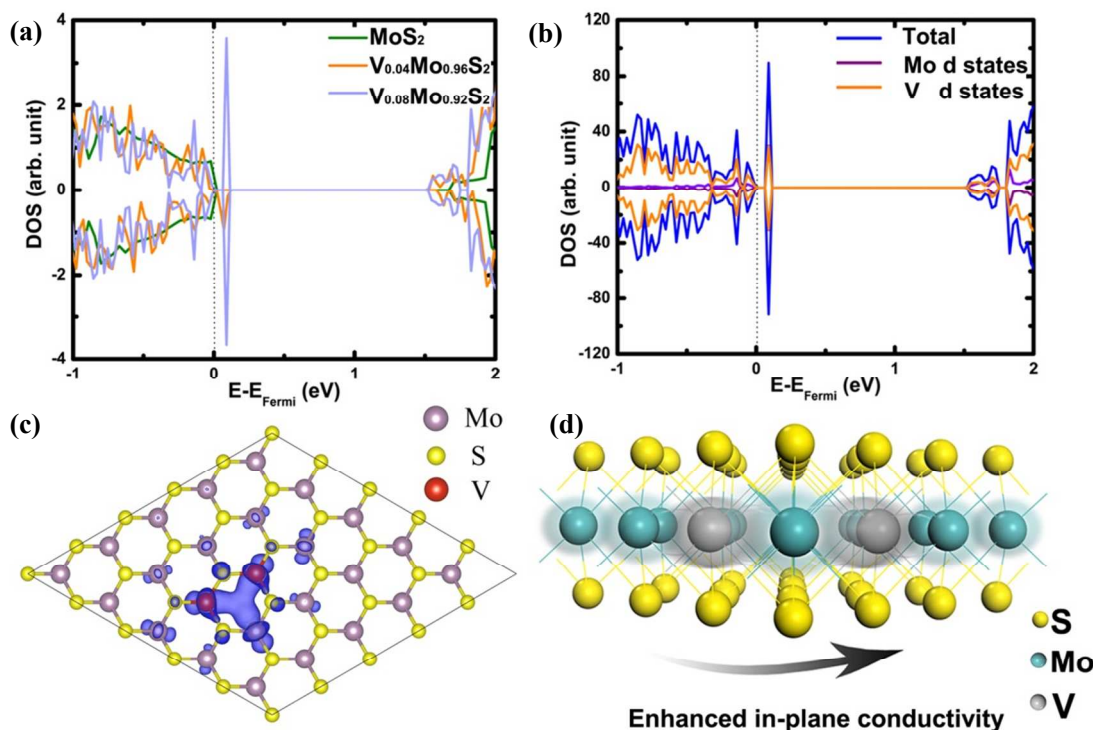
Figure 1. (a) DOS diagrams for single-layered VMS with various Mo/V ratios and the pure MoS_2 nanosheet calculated by PBE functional, revealing the distinct transport properties of these samples. (b) DOS diagram of $V_{0.08}Mo_{0.92}S_2$ nanosheet. (c) Isosurface (blue area) of the empty state above the Fermi level of $V_{0.08}Mo_{0.92}S_2$ with an isovalue of 0.002 e/au, purple, yellow and red spheres denote Mo, S and V atoms, respectively. (d) Schematic illustration of the enhanced in-plane conductivity due to the incorporated vanadium atoms.
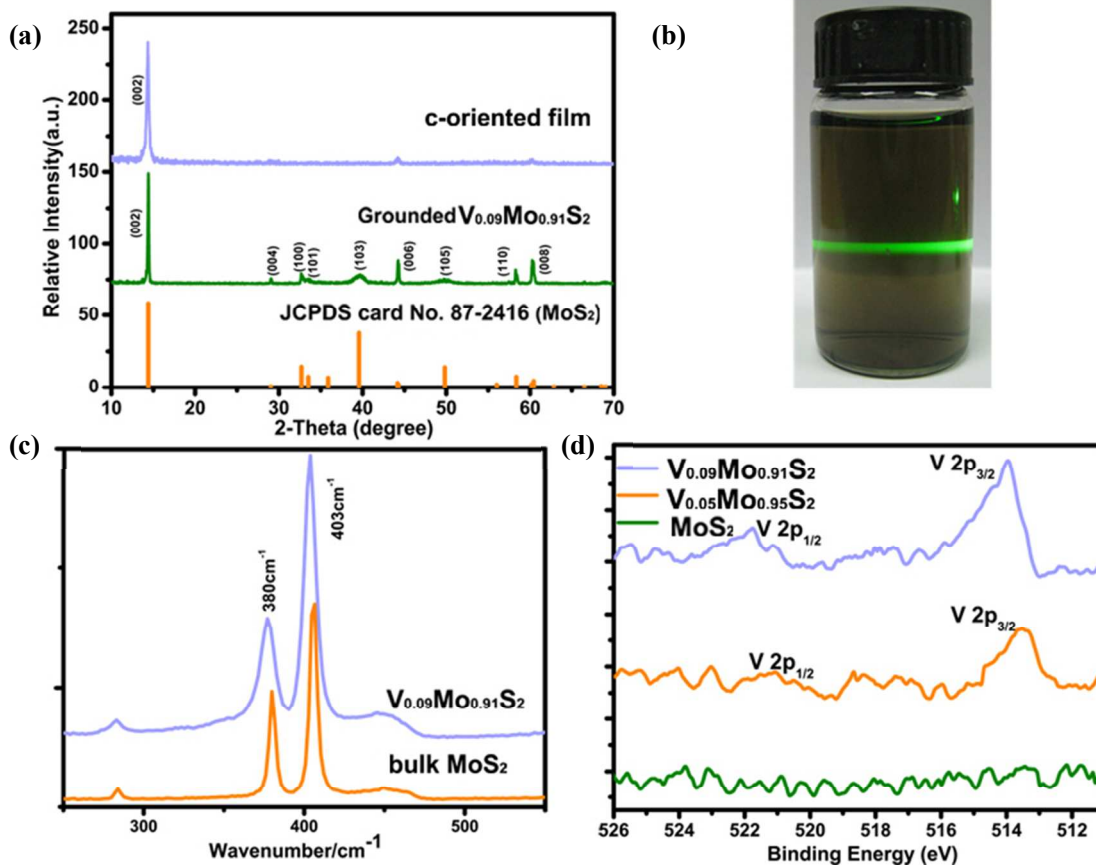
Figure 2. (a) The XRD patterns of the synthesized vanadium-doped MoS_2 with 2H structure and the as-assembled VMS with well-defined c-orientation; (b) Tyndall effect of the VMS nanosheet solution; (c) The Raman spectra of the assembled film of VMS nanosheets; (d) Representative V 2p XPS spectra of pure MoS_2 and VMS samples with different Mo/V ratios.

semimetal behavior in a broad temperature range, rather than the Mott-insulator character as that in pure MoS_2 system. The as-achieved VMS ultrathin nanosheets possess the significantly enhanced in-plane conductivity (1.7×10^3 S/m at 280 K) and a higher carrier concentration (7×10^{17} cm^{-3}), which is about 40 times and 20 times larger than that for pure MoS_2 system (40 S/m and 3.5×10^{16} cm^{-3})[24], respectively. Moreover, considering the reduced catalytic efficiencies due to the inferior electron transferring between two S-Mo-S layers in the bulk MoS_2, the VMS nanosheets with graphene-like structure afford an advanced electron transfer path between in-plane overlapped nanosheets two-dimensionally and thus avoid 3D inferior transfer process between layers in bulk MoS_2. Benefited from the enhanced in-plane conductivity, improved carrier concentrations as well as the shortened electron transfer paths, the semimetallic VMS nanosheet exhibited the enhanced catalytic properties compared with pure MoS_2 system, pointing the new way toward high efficiency catalysts in materials with graphene-like structure.

Experimental Section

Preparation of the bulk vanadium-doped MoS_2 with different ratios: Raw bulk V-doped MoS_2 precursors with gradual increasing Mo/V ratios are synthesized by the solid state reaction with a mixture of vanadium, molybdenum and sulfur

powders at high temperature. All the samples were mixed uniformly and then loaded into a fused silica tube. The tube was evacuated to 10^{-3} Torr and flame-sealed. It was then held at 900 °C for 12 h, followed by cooling to 20 °C over 36 h. Pure MoS_2 precursor was synthesized via the solid reaction with a mixture of molybdenum and sulfur powders as other conditions are the same.

Exfoliation of the precursor into VMS nanosheets: To prepare high-quality VMS nanosheets solution, we adopted a recently developed liquid exfoliation method, that is, to exfoliate layered compounds in specific organic solvents.[25] Due to the matched surface energy between the solvent and ultrathin nanosheet, N-methyl-pyrrolidinone (NMP) was adopted as an exfoliation solvent. In our experiment, 20 mg bulk VMS was dispersed in a conical flask with 30 ml NMP and then bubbled with argon to expel the dissolved oxygen away from the solution. Then the obtained solution was sonicated for 5 hours. Then a well dispersed VMS nanosheets solution was achieved. And the as-obtained VMS nanosheets solution kept stability for several weeks. For a comparison, pure MoS_2 nanosheet was obtained via the same way as being exfoliated in NMP.

Assembly of VMS nanosheets into transferrable thin films: To study the structure details of the exfoliated nanosheets, a compacted film was fabricated and transferred onto a silicon wafer. In detail, the VMS nanosheet solution was vacuum-filtrated over a cellulose membrane with 0.22 μm pore size to
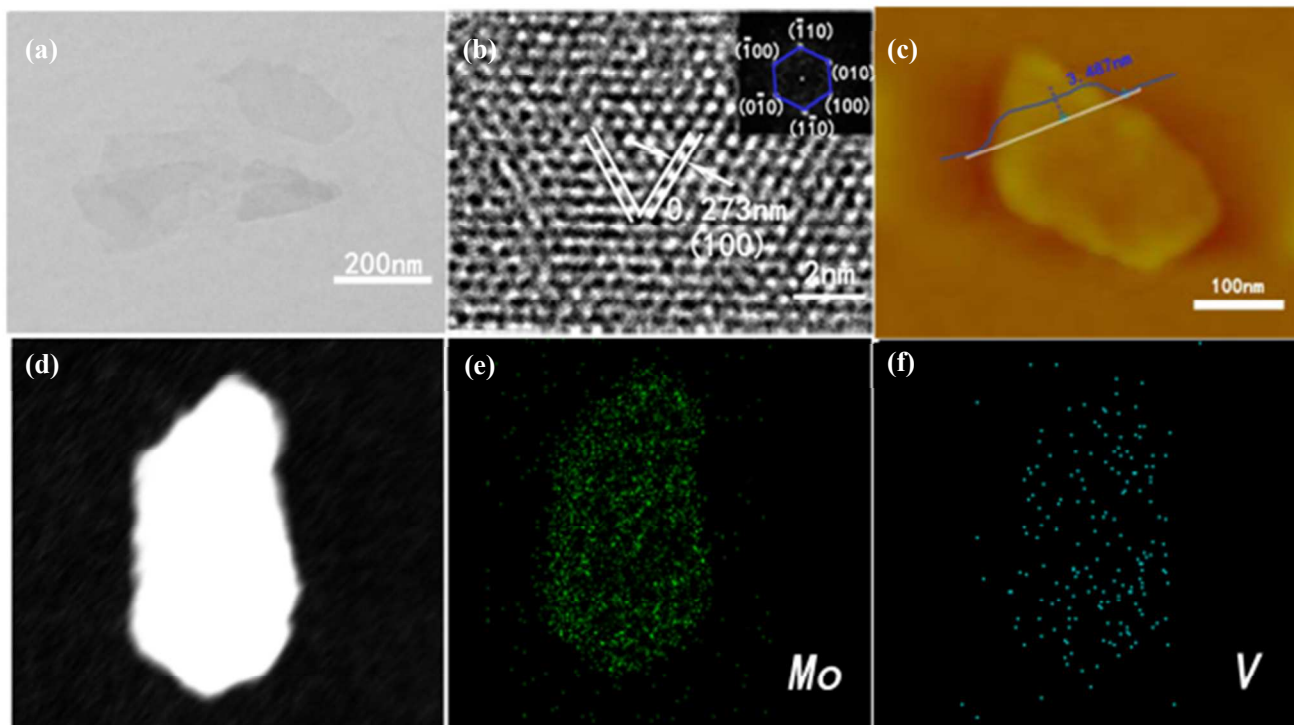
Figure 3. Ultrathin vanadium-doped MoS_2 nanosheets (a) TEM image; (b) HRTEM image of a typical nanosheet, inset: the corresponding fast Fourier transform pattern (c) Tapping mode AFM image; (d) The HADDF-STEM image; (e) and (f) EDS mapping of Mo and V of nanosheet, respectively.

form a homogeneous thin film, of which the thickness can be tuned by changing the filtrated amount of VMS nanosheet solution. Then the X-ray diffraction (XRD) was employed to reveal the orientation of this restacked film.

Electrochemical measurements: 4 mg of catalysts (VMS nanosheet, pure MoS_2 nanosheet or pure bulk MoS_2) and 40 μl of 5 wt% Nafion solution were dispersed in 1 ml water/ethanol with a v/v of 3:1. After sonication for 30 min, a homogeneous ink was achieved. Then 5 μl of the above catalyst ink was loaded onto a glassy carbon electrode of 3mm in diameter (loading 0.285 mg/cm^2). In order to make a comparison, the bare glassy carbon electrode was also polished and cleaned for electrochemical measurement. The reference was an Ag/AgCl (3 mol/L KCl) electrode and the counter electrode was graphite rod electrode. All the potentials in our manuscript are reported vs. the reversible hydrogen electrode (RHE) based on the Nernst equation. Polarization curves were obtained by linear sweep voltammetry with a scan rate of 2 mVs-1 on electrochemical station (CHI 660B) in Ar-saturated 1M H_2SO_4. AC impedance measurements of the VMS catalyst were carried out in the same configuration at η = 0.22 V from 100 kHz to 5 mHz with the applied voltage of 5 mV with a Zahner IM6 electrochemical workstation in Ar-saturated 1M H_2SO_4. To evaluate the stability of the catalyst, the tests were performed in Ar-saturated 1 M H_2SO_4 at room temperature by potential cycling between -0.6 and 0.2 V vs. Ag/AgCl at a sweep rate of 100 mVs^{-1} for about 1000 cycles. At the end of cycling, the resulting electrode was used for polarization curves.

Calculation Details: Electronic structure calculations and geometrical optimizations are performed using density-functional theory as implemented in VASP 5.3.[26] The exchange-correlation energy is treated using the PBE-type

GGA functional. The ion-electron interaction is treated using the projector augment wave (PAW) technique. For geometric optimization, both lattice constants and atomic positions are relaxed until the forces on atoms are less than 0.02 eV/Å and the total energy change is less than 1.0×10^{-5} eV. The Brillouin zone is sampled using k-points with 0.02 Å^{-1} spacing in the Monkhorst-Pack scheme for geometry optimization, and for density of states (DOS) calculations,[27] a denser grid with 0.01 Å^{-1} spacing is used. To approach the synthesized V:Mo ratios with a balance of accuracy and efficiency, 5×5 MoS_2 supercells with one Mo and two Mo atom substituted by V atoms are adopted, corresponding to $V_{0.04}Mo_{0.96}S_2$ and $V_{0.08}Mo_{0.92}S_2$. In the case of $V_{0.08}Mo_{0.92}S_2$, different possible substitution sites of V are tested, and the one with lowest energy is used for discussion.

Characterizations: X-ray diffraction (XRD) were performed on a Philips X'Pert Pro Super diffractometer with Cu Ka radiation (λ = 1.54178 Å). The transmission electron microscopy (TEM) images were obtained on a JEOL-2010 transmission electron microscope at an acceleration voltage of 200 kV. X-ray photoelectron spectra (XPS) were acquired on an ESCALAB MK II with Mg Ka as the excitation source. Raman spectra were recorded at room temperature with a LABRAM-HR Confocal Laser Micro Raman Spectrometer 750 K with a laser power of 0.5 mW. The field emission scanning electron microscopy (FE-SEM) images were taken on a JEOL JSM-6700F SEM. Scanning transmission electron microscopy (STEM) images, energy dispersive X-ray spectrums (EDS) were obtained on a JEM 2100F (field emission) transmission electron microscopes equipped with an Oxford INCA x-sight EDS Si(Li) detector at an acceleration voltage of 200 kV. The electrical transport property measurements were carried out
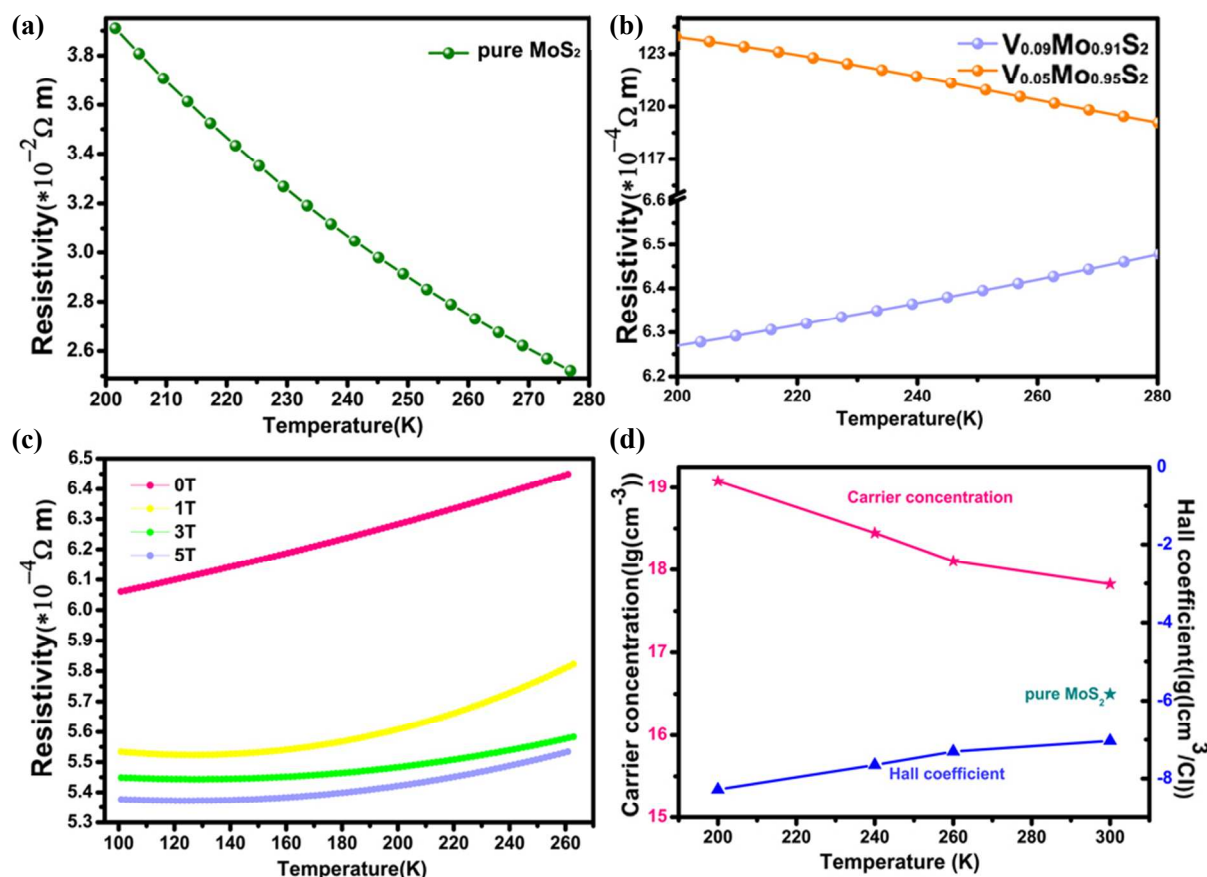
Figure 4. Unique half metallic behavior of vanadium doped MoS_2. Temperature dependence of resistivity of MoS_2 (a) and V-MoS_2 with different V / Mo ratios (b). (c) Temperature-dependent electrical resistivity for $V_{0.09}Mo_{0.91}S_2$ under various magnified field. (d) Temperature dependent of carrier concentration and Hall coefficient of $V_{0.09}Mo_{0.91}S_2$.

using a Keithley 4200-SCS Semiconductor Characterization System and a four-point probe method. Hall coefficient and magnetoresistance were measured by a four-probe technique using a Quantum Design Physical Property Measurement System (PPMS)-9 using the van der Pauw method.

Results and discussion

Intralayer vanadium doped MoS_2 (VMS) samples with gradual increasing V/Mo ratios were synthesized by the solid state reaction with a mixture of vanadium, molybdenum and sulfur powders. The VMS ultrathin nanosheets with few atomic layers were obtained by the liquid exfoliation method due to the surface energy matching between the solvent and ultrathin nanosheet.[25] The inductively coupled plasma (ICP) analysis gives the molecular formula as $V_{0.09}Mo_{0.91}S_2$ and $V_{0.05}Mo_{0.95}S_2$, respectively. A compacted film was also prepared by the vacuum-filtration method for further study of the structure of the exfoliated nanosheets. The experimental details are shown in supporting information. The XRD patterns (Figure 2a and Figure S3) of the synthesized $V_{0.09}Mo_{0.91}S_2$ can be well indexed to MoS_2 (JCPDS, No.87-2416) with diffraction peaks gradually shifted to a higher diffraction angle as part of Mo were substituted by V. As for the diffraction patterns of the assembled film, only the lattice planes with equally spaced

indexes of (00l) were detected, suggesting the highly c-axis orientation of the assembled film. Meanwhile, Raman spectra of pure bulk MoS_2 and the assembled film of VMS nanosheet (Figure 2c) were measured to further confirm the well maintained 2H S-(V, Mo)-S structure after doping and exfoliation. Two prominent peaks corresponding to the in-plane E^1_{2g} (380cm^{-1}) and out-of-plane A_{1g} (403 cm^{-1}) modes of 2H-MoS2 that map exactly onto the previous literature spectra[28] of 2H-MoS_2 can be clearly seen in both samples with no other vibration peaks arising. The frequency difference between E^1_{2g} and A_{1g} is about 23cm^{-1}, a little smaller than bulk MoS_2, which is in consistence with the previous literature.[29] Also, the A_{1g} and E^1_{2g} modes in VMS nanosheet softened with larger full widths at half maximum values (11-12 cm^{-1}) than bulk MoS_2 (3 cm^{-1}), which should be attributed to the phonon confinement in these two dimensional nanosheet. The above results demonstrated that the pristine 2H lattice structure was maintained after vanadium doping as well as exfoliation. Moreover, elemental ingredients of the involving of vanadium in VMS nanosheets were revealed by the X-ray photoelectron spectroscopy (XPS) analysis. The V2p peaks in the XPS spectra of VMS samples with various V/Mo ratios denoted as $V_{0.09}Mo_{0.91}S_2$ and $V_{0.05}Mo_{0.95}S_2$, were shown in Figure 2d. It can be seen that the peaks appearing at 513 eV~514 eV corresponded to V $2p_{3/2}$. In a word, careful characterization

verified the common 2H-MoS$_2$ polymorph in our VMS sample with vanadium atoms incorporating into the basal plane.

exfoliated into ultrathin nanosheets of good quasi-2D crystallinity with microscopic orientation along c axis.
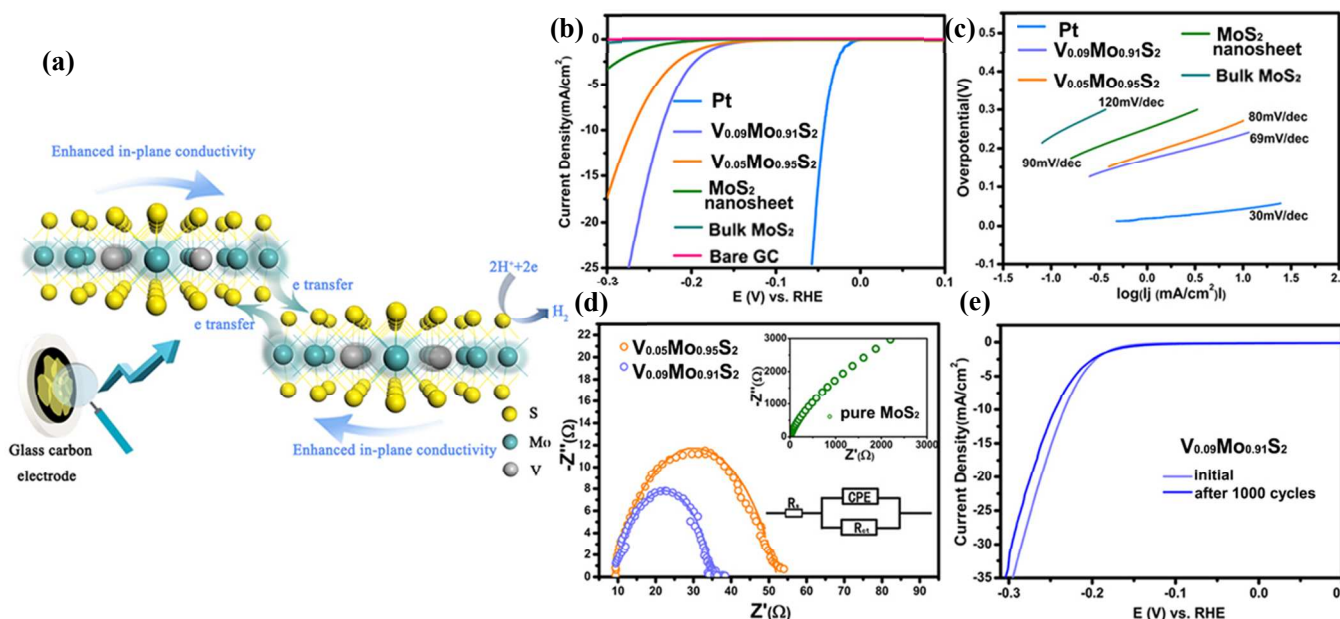
Figure 5. (a) Schematic illustration of the enhanced catalytic activity of the VMS nanosheet catalysts due to the enhanced in-plane conductivity via vanadium doping and the improved electron transfer between the overlapped nanosheet edges triggered by their metallic nature based on the calculation results. (b) Polarization curves recorded on decorated GC electrode consisting of various VMS nanosheet catalysts and commercial MoS$_2$. (c) The corresponding Tafel plots derived from (b). (d) Nyquist plot of the VMS nanosheet catalysts. Z' is real impedance and Z'' is imaginary impedance. Inset: The Nyquist plot of pure MoS$_2$ nanosheet catalyst and the equivalent circuit of the EIS spectroscopy. The empty circles represent the experimental data and the solid line is the fitted curve. (e) Durability test for the V$_{0.09}$Mo$_{0.91}$S$_2$ catalyst.

Microscopic characterization further verified the ultrathin character of the 2H-VMS nanosheets. Transmission electron microscopy (TEM) image (Figure 3a) shows the free-standing nanosheets with lateral size about 200 nm. The high-resolution TEM (HRTEM) investigation and fast Fourier transform pattern (Figure 3b) performed on a typical ultrathin nanosheet reveal the single-crystalline nature of the as-exfoliated nanosheet. The interplanar distance of 2.73Å corresponded to the (100) and (010) lattice plane of the MoS$_2$ crystal structure, demonstrated that the vanadium containing nanosheet was exfoliated along the c-direction. Meanwhile, the interplane angle of 60° of the two planes of (010) and (100) in the fast Fourier transform pattern as well as the well-defined hexagonal symmetry without additional points was fairly consistent with those calculated from hexagonal crystal graphic parameters of 2H-MoS$_2$, confirming the well-kept 2H structure of VMS nanosheet. Tapping mode atomic force microscopy (AFM) (Figure 3c) was performed to evaluate the thickness of the VMS nanosheets. Prominently, the thickness was measured to be about 3.5nm, corresponding to about five S-(V, Mo)-S atomic layers, in that the c parameter of 2H-MoS$_2$ is 6.2Å, demonstrating the successful exfoliation of VMS nanosheets with high quality and quasi-2D crystallinity. The thickness distribution of VMS nanosheet was shown in Figure S8. Typical HAADF-STEM and elemental mapping images of an exfoliated VMS nanosheet were presented in Figure 3d-f, from which the homogenously spatial distributions of Mo (indicated by green color) and V (indicated by blue color) in the nanosheet were clearly observed, demonstrating the uniform distribution of vanadium atoms among the whole sheet. The above results clearly demonstrated that the VMS samples were successfully

To demonstrate the influence of the incorporation of V atoms on the electronic behavior of layered MoS$_2$, measurements of the temperature dependent resistivity of pure MoS$_2$ and VMS samples were carried out, as shown in Figure 4a and b. With the change of temperature, distinctive behaviors were observed among these samples. The resistivity of pure MoS$_2$ and V$_{0.05}$Mo$_{0.95}$S$_2$ decreased with increasing temperature, manifesting a typical semiconductor characteristic. However, the resistivity of V$_{0.05}$Mo$_{0.95}$S$_2$ is much smaller than that of pure MoS$_2$, verifying that the incorporated vanadium atoms indeed improved the electrical conductivity. In sharp contrast, an increasing response of resistivity was displayed in V$_{0.09}$Mo$_{0.91}$S$_2$ specimen along with the increment of temperature, manifesting the semimetallic conducting behavior. The obviously distinct behaviors among these samples are attributed to the fine regulation of the intrinsic electronic structure by the intralayer-doped vanadium atoms as demonstrated in our DFT calculations (Figure 1a and b). For the sample with lower V/Mo ratio (V$_{0.04}$Mo$_{0.96}$S$_2$), the incorporation of V resulted in a defect state in the spin down channel, while the gap almost remains the same in the spin up channel. Since the behaviors of the temperature dependent resistivity between the two spin channels are competitive with each other, the sample exhibits a half-semimetallic behavior with a better conductivity than pure MoS$_2$ sample. Moreover, for the higher V/ Mo ratio (V$_{0.08}$Mo$_{0.92}$S$_2$), the interaction between the incorporated V atoms and neighbor Mo atoms (see Figure 1c and d) introduced defect states in both spin channels. The small energy difference between the defect states and the top of the valence band makes it easier for the activation of the valence electrons. At very low temperature, the carrier density increases with the temperature

increasing until it reaches saturation state at a certain temperature. Then the conductivity of the sample is mainly controlled by the interactions between the electrons and phonons, similar to that of metal, behaving the semimetallic character as shown in Figure 4b.

Meanwhile, the temperature dependence of the resistivity was also performed under various magnetic fields as shown in Figure 4c, from which the semimetallic conductivity was further demonstrated as the resistivity increased along the increment of the temperature. The negative magnetoresistance here also illustrates the probable existence of magnetism resulted by the vanadium insertion in the pristine nonmagnetic MoS_2. The Hall coefficient characterization (Figure 4d) revealed that the carrier concentration was increased by a factor of 20 times at room temperature compared with the reported value of pure MoS_2 (marked with pentagram in Figure 4d)[23], demonstrating that the vanadium insertion indeed influence the intrinsic physical properties of MoS_2. Meanwhile, the negative Hall coefficients were in consistence with the spin-polarized behavior with the carriers of electrons.

Since the electron transfer process for catalysts is the key step in the catalytic reaction, the enhanced conductivity, high carrier concentration and the optimized electron transfer paths would be the desirable characteristics for an ideal catalyst. Meanwhile, compared with the phase transition caused by the alkaline metal insertion, the intralayer vanadium doping caused no phase changes with the stable 2H structure well kept, which is of great advantages in the electrochemical environment. Quantum-mechanical calculations reveal that the proper bonding strength (ΔE_S) of sulphur at the metallic edges makes single layer MoS_2 catalytically active. Thus, the realization of enhanced conductivity and high carrier concentration brought by the stable semimetallic character in VMS nanosheets as schematically illustrated in Figure 5a, is meaningful for the intriguing application as a catalyst for HER.

To investigate the electrocatalytic HER activity of VMS nanosheets, glassy carbon electrodes modified with either VMS nanosheets or pure MoS_2 were prepared for cyclic voltammetry (CV) in Ar-saturated 1M H_2SO_4. As a reference, the similar measurements were also performed on bare glassy-carbon electrode (GC) and commercial Pt/C catalyst (20 wt % Pt on Vulcan carbon black). As presented in the polarization curve (Figure 5b), the onset potential of the VMS nanosheets is about -0.13 V, beyond which the current rose rapidly under more negative potentials. In sharp contrast, the onset potential of pure MoS_2 system (both pure MoS_2 nanosheet and pure bulk MoS_2) shifts to more negative value, illustrating a much inferior HER activity. Considering the polarization current, it is of note that the exfoliated VMS samples exhibited an obvious increasing current density than pure MoS_2 system (Table S3). The evident current differences among these samples are in consistent with their various electrical properties, that is, with more doped vanadium atoms, the semimetallic conductivity was achieved with enhanced electrical conductivity and carrier concentrations. The Tafel plots, which are often adopted to analyze quantitative kinetics, are shown in Figure 5c. The Tafel slopes were calculated to be ~69 and ~80 mV/decade for nanosheets catalysts of $V_{0.09}Mo_{0.91}S_2$ and $V_{0.05}Mo_{0.95}S_2$ respectively, which were obvious lower than pure MoS_2 nanosheet (90 mV/dec) and bulk MoS_2 catalyst (120 mV/dec). In consideration of the uncompensated solution resistance, iR correction was performed (Figure S17 and S18), after which the Tafel slopes were reduced to 60mV/dec and 75mV/dec for

$V_{0.09}Mo_{0.91}S_2$ and $V_{0.05}Mo_{0.95}S_2$ respectively, revealing even more enhanced catalytic activity than pure MoS_2.

Since the electrochemical impedance spectroscopy (EIS) is often applied to study the electrode kinetics in HER process,[30] AC impedance measurement was performed over the frequency range at η = 0.22 V from 100 kHz to 5mHz for the investigation of the catalytic kinetics of the VMS catalyst. The equivalent circuit and detailed analysis were shown in Figure S17. As can be seen from the semicircle in the the Nyquist plot (Figure 5d), the vanadium doped MoS_2 catalysts show much smaller charge transfer resistance (26.05 Ω for $V_{0.09}Mo_{0.91}S_2$ and 43.89 Ω for $V_{0.05}Mo_{0.9}5S_2$) than pure MoS2 (2.7 kΩ), presenting the much faster electron transfer process. And in our system, the charge transfer resistance decreased significantly with increasing overpotentials as previously reported[29], varying from 105 Ω to 17.74 Ω along with the increment of the overpotential from 180mV to 250 mV (Figure S19). The EIS result suggests that the intralayer-doped vanadium atoms indeed optimized the electrical properties in MoS_2 system, thus leading to the much faster electron transfer process.

The high durability is another desired criterion for an advanced electrocatalyst. To evaluate its durability, the $V_{0.09}Mo_{0.91}S_2$ catalyst was cycled continuously for 1000 cycles (Figure 5e). Only a slight activity loss was observed at the end of the cycling, demonstrating that the VMS catalyst is of superior stability in a long-term electrochemical process. Meanwhile, continuous HER at static overpotential (200mV) was also conducted to demonstrate the stability. The time-dependent curve is shown in Figure S20, from which the continuous HER process was observed, illustrating the high stability of the VMS catalyst.

With intralayer vanadium doping in 2D MoS_2 lattice framework, fine modulation of the intrinsic properties indeed enhanced the catalytic efficiency of MoS_2 material system. Compared with pure MoS_2, the VMS nanosheets catalysts exhibited an increased catalytic property. We attributed the high performance of our VMS nanosheets catalyst in HER to the enhanced electrical conductivity and higher carrier concentration. With the vanadium incorporation, the arisen semimetallic character in VMS has led to the enhanced conductivity (1.7×10^3 S/m) and higher carrier concentration (7×10^{17} cm^{-3}), which is about 40 times and 20 times larger than that for pure MoS_2 system, respectively. Meanwhile, the nanosheet structure also avoids the 3D inferior transfer process between layers in bulk MoS_2, thus affording a rapid electron transfer as well. As a fact, the smaller charge transfer resistance as shown in Figure 5d provides forceful evidence for the realization of a much faster electron transfer process during the hydrogen evolution process.

Conclusions

In conclusion, we demonstrated an intralayer doping strategy to successfully regulate the intrinsic physical properties of MoS_2 within its pristine 2H structure. Our obtained vanadium-doped MoS_2 represents a new intralayer-doped TMD material in MoS_2 material system, ensuring the efficient exfoliation into $V_xMo_{1-x}S_2$ ultrathin nanosheets with less than 5 S-(V, Mo)-S atomic layers as a new 2D inorganic material. Unlike the Mott-insulator of pure MoS_2 sample, our VMS ultrathin nanosheet behaves semimetal character, as new semimetallic MoS_2 with graphene-like structure, with a significantly enhanced electrical conductivity (1.7×10^3 S/m at 280 K) and a higher carrier

concentration (7×10^{17} cm^{-3}), which are about 40 times and 20 times larger than that for pure MoS_2 system (40 S/m and 3.5×10^{16} cm^{-3}), respectively. Benefited from the enhanced electrical properties as well as the 2D in-plane conducting paths which avoided the inferior inner 3D electron transfer, the VMS semimetallic nanosheet brought an enhanced catalytic activity with the overpotential of 0.13V and a smaller Tafel slope, exhibiting significantly enhanced catalytic performance than that of pure MoS_2 system. The intralayer doping in 2D structure provides a new avenue to construct advanced 2D catalysts for high efficiency energy conversion and to greatly enlarge the design space of 2D materials.

Acknowledgements

Notes and references

^{a} Hefei National Laboratory for Physical Sciences at Microscale,
University of Science and Technology of China, Hefei 230026, P. R. China, E-mail: czwu@ ustc.edu.cn
^{b} Department of Chemistry,
University of Nebraska-Lincoln, Lincoln, Nebraska, 68588, United States
†Electronic Supplementary Information (ESI) available. See DOI: 10.1039/b000000x/

1 (a) N. S. Lewis, D. G. Nocera, *Proc. Natl Acad. Sci. U. S. A.* 2006, **103**, 15729; (b) J. A. Turner, *Science* 2004, **305**, 972; (c) M. S. Dresselhaus, I. L. Thomas, *Nature* 2001, **414**, 332.

2 (a) E. S. Andreiadis, P.-A. Jacques, P. D. Tran, A. Leyris, M. Chavarot-Kerlidou, B. Jousselme, M. Matheron, J. Pécaut, S. Palacin, M. Fontecave, V. Artero, *Nat. Chem.* 2013, **5**, 48; (b) R. Subbaraman, D. Tripkovic, D. Strmcnik, K.-C. Chang, M. Uchimura, A. P. Paulikas, V. Stamenkovic, N. M. Markovic, *Science* 2011, **334**, 1256; (c) M. L. Helm, M. P. Stewart, R. M. Bullock, M. R. DuBois, D. L. DuBois, *Science* 2011, **333**, 863.

3 (a) K. Tedsree, T. Li, S. Jones, C. W. A. Chan, K. M. K. Yu, P. A. J. Bagot, E. A. Marquis, G. D. W. Smith, S. C. E. Tsang, *Nat. Nano.* 2011, **6**, 302-307; (b) M. Smiljanić, I. Srejić, B. Grgur, Z. Rakočević, S. Štrbac, *Electrchem. Commun.* 2013, **28**, 37-39.

4 (a) T. Zhu, H. B. Wu, Y. B. Wang, R. Xu, X. W. Lou, *Adv. Energy Mater.* 2012, **2**, 1497; (b) D. Voiry, H. Yamaguchi, J. Li, R. Silva, D. C. B. Alves, T. Fujita, M. Chen, T. Asefa, V. B. Shenoy, G. Eda, M. Chhowalla, *Nat. Mater.* 2013, **12**, 850.

5 (a) J. V. Lauritsen, J. Kibsgaard, S. Helveg, H. Topsoe, B. S. Clausen, E. Laegsgaard, F. Besenbacher, *Nat. Nano.* 2007, **2**, 53-58; (b) T. F. Jaramillo, K. P. Jørgensen, J. Bonde, J. H. Nielsen, S. Horch, I. Chorkendorff, *Science.* 2007, **317**, 100-102; (c) H. I. Karunadasa, E. Montalvo, Y. Sun, M. Majda, J. R. Long, C. J. Chang, *Science.* 2012, **335**, 698-702. (d) J. Xie, H. Zhang, S. Li, R. X. Wang, X. Sun, M.

6 S. Trasatti, *J. Electroanal. Chem. Interfac.* 1971, **33**, 351.

7 J. Kibsgaard, Z. Chen, B. N. Reinecke, T. F. Jaramillo, *Nat. Mater.* 2012, **11**, 963.

8 X. Huang, Z. Y. Zeng, S. Y. Bao, M. F. Wang, X. Y. Qi, Z. X. Fan, H. Zhang, *Nat. Commun.* 2013, **4**, 1444.

9 D. S. Kong, H. T. Wang, J. J. Cha, M. Pasta, K. J. Koski, J. Yao, Y. Cui, *Nano Letters.* 2013, **13**, 1341.

10 J. Kim, S. Byun, A. J. Smith, J. Yu, J. X. Huang, *J. Phys. Chem. Lett.* 2013, **4**, 1227.

11 Y. G. Li, H. L. Wang, L. M. Xie, Y. Y. Liang, G. S. Hong, H. J. Dai, *J. Am. Chem. Soc.* 2011, **133**, 7296.

12 T. Y. Wang, L. Liu, Z. W. Zhu, P. Papakonstantinou, J. B. Hu, H. Y. Liu, M. X. Li, *Energy Environ. Sci.* 2013, **6**, 625.

13 M. A. Lukowski, A. S. Daniel, F. Meng, A. Forticaux, L. S. Li, S. Jin, *J. Am. Chem. Soc.* 2013, **135**, 10274.

14 M. V. Bollinger, J. V. Lauritsen, K. W. Jacobsen, J. K. Nørskov, S. Helveg, F. Besenbacher, *Phys. Rev. Lett.* 2001, **87**, 196803.

15 (a) M. Chhowalla, H. S. Shin, G. Eda, L.-J. Li, K. P. Loh, H. Zhang, *Nat. Chem.* 2013, **5**, 263-275; (d) X. Huang, Z. Y. Zeng, H. Zhang, *Chem. Soc. Rev.* 2013, **42**, 1934;

16 (a) Y. F. Sun, Z. H. Sun, S. Gao, H. Cheng, Q. H. Liu, F. C. Lei, S. Q. Wei, Y. Xie, *Adv. Energy Mater.* 2013, DOI: 10.1002/aenm.201300611; (b) C. W. Lin, X. J. Zhu, J. Feng, C. Z. Wu, S. L. Hu, J. Peng, Y. Q. Guo, L. L. Peng, J. Y. Zhao, J. L. Huang, J. L. Yang, Y. Xie, *J. Am. Chem. Soc.* 2013, **135**, 5144. (c) Y. F. Sun, H. Cheng, S. Gao, Z. H. Sun, Q. H. Liu, Q. Liu, F. C. Lei, T. Yao, J. F. He, S. Q. Wei, Y. Xie, *Angew. Chem. Int. Ed.* 2012, **57**, 8727; (d) J. Feng, X. Sun, C. Z. Wu, L. L. Peng, C. W. Lin, S. L. Hu, J. L. Yang, Y. Xie, *J. Am. Chem. Soc.* 2011, **133**, 17832.

17 RadisavljevicB, RadenovicA, BrivioJ, GiacomettiV, KisA, *Nat. Nano* 2011, **6**, 147

18 (a) J. T. Ye, Y. J. Zhang, R. Akashi, M. S. Bahramy, R. Arita, Y. Iwasa, *Science.* 2012, **338**, 1193-1196; (b) K. Taniguchi, A. Matsumoto, H. Shimotani, H. Takagi, *Appl. Phys. Lett.* 2012, **101**, 042603.

19 L. F. Mattheiss, *Phys. Rev. B* 1973, **8**, 3719.

20 A. Zak, Y. Feldman, V. Lyakhovitskaya, G. Leitus, R. Popovitz-Biro, E. Wachtel, H. Cohen, S. Reich, R. Tenne, *J. Am. Chem. Soc.* 2002, **124**, 4747.

21 M. A. Py, R. R. Haering, *Can. J. Phys.* 1983, **61**, 76.

22 D. Yang, S. J. Sandoval, W. M. R. Divigalpitiya, J. C. Irwin, R. F. Frindt, *Phys. Rev. B* 1991, **43**, 12053.

23 (a) C. Z. Wu, F. Feng, Y. Xie, Chem. Soc. Rev, 2013, 42, 5157-5183; (b) C. Z. Wu, Y. Xie, *Energy Environ. Sci.*, 2010, **3**, 1191-1206.

24 S. H. El-Mahalawy, B. L. Evans, *phys. Stat. sol.* (b) 1977, **79 (2)**, 713.

25 J. N. Coleman, M. Lotya, A. O'Neill, S. D. Bergin, P. J. King, U. Khan, K. Young, A. Gaucher, S. De, R. J. Smith, I. V. Shvets, S. K. Arora, G. Stanton, H.-Y. Kim, K. Lee, G. T. Kim, G. S. Duesberg, T. Hallam, J. J. Boland, J. J. Wang, J. F. Donegan, J. C. Grunlan, G. Moriarty, A. Shmeliov, R. J. Nicholls, J. M. Perkins, E. M. Grieveson, K. Theuwissen, D. W. McComb, P. D. Nellist, V. Nicolosi, *Science* 2011, **331**, 568.

26 (a) G. Kresse, J. Furthmüller, *J. Comput. Mater. Sci.* 1996, 6, 15; (b) G. Kresse, J. Furthmüller, *J. Phys. Rev. B* 1996, **54**, 11169..

Zhou, J. F. Zhou, X. W. Lou, Y. Xie, *Adv. Mater.*2013, DOI. 10.1002/adma.201302685

27 H. J. Monkhorst, J. D. Pack, *Phy. Rev. B* 1976, **13**, 5188.

28 Z. Y. Zeng, Z. Y. Yin, X. Huang, H. Li, Q. Y. He, G. Lu, F. Boey, H. Zhang, *Angew. Chem. Int. Ed.* 2011, **50**, 11093.

29 (a) H. Li, Q. Zhang, C. C. R. Yap, B. K. Tay, T. H. T. Edwin, A. Olivier, D. Baillargeat, *Adv. Funct. Mater.* 2012, **22**, 1385. (b) C. N. R. Rao, H. S. S. Ramakrishna Matte, U. Maitra, *Angew. Chem. Int. Ed.* 2013, DOI: 10.1002/anie.201301548.

30 (a) D. Merki, H. Vrubel, L. Rovelli, S. Fierro, X. L. Hu, *Chem. Sci.* 2012, **3**, 2515; (b) L. Liao, J. Zhu, X. J. Bian, L. N. Zhu, M. D. Scanlon, H. H. Girault, B. H. Liu, *Adv. Funct. Mater.* 2013, DOI: 10.1002/adfm.201300318.

Nanoscale Accepted Manuscript

Nanoscale

ARTICLE

TOC figure
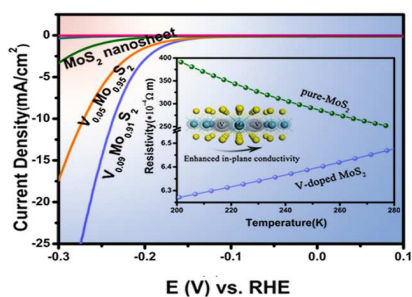
Intralayer vanadium doped $V_xMo_{1-x}S_2$ ultrathin nanosheets, has led to novel semimetallic behavior with significantly enhanced conductivity (1.7×10^3 S/m) and carrier concentration (7×10^{17} cm^{-3}).